

Astrophysical interpretation of small-scale neutrino angular correlation searches with IceCube

Martin Leuermann^a, Michael Schimp^{a,b,*}, Christopher H. Wiebusch^a

^a*III. Physikalisches Institut B, RWTH Aachen University, Aachen, Germany*

^b*Now at Bergische Universität Wuppertal, Fachbereich C – Physik, Wuppertal, Germany*

Abstract

The IceCube Neutrino Observatory has discovered a diffuse all-flavor flux of high-energy astrophysical neutrinos. However, the corresponding astrophysical sources have not yet been identified. Neither significant point sources nor significant angular correlations of event directions have been observed by IceCube or other instruments to date. We present a new method to interpret the non-observation of angular correlations in terms of exclusions on the strength and number of point-like neutrino sources in generic astrophysical scenarios. Additionally, we constrain the presence of these sources taking into account the measurement of the diffuse high-energy neutrino flux by IceCube. We apply the method to two types of astrophysically motivated source count distributions: The first type is obtained by considering the cosmological evolution of the co-moving density of active galaxies, while the second type is directly derived from the gamma ray source count distribution observed by Fermi-LAT. As a result, we constrain the possible parameter space for both types of source count distributions.

Keywords: Neutrino astronomy, IceCube, Cosmic neutrino sources

1. Introduction

1.1. Astrophysical neutrino observation by IceCube

The IceCube Neutrino Observatory [7] at the Geographic South Pole has discovered an all-sky diffuse flux of high-energy cosmic neutrinos [2, 1] based on neutrinos of all flavors interacting within the detector. However, no astrophysical sources of this flux could be identified yet. Recently, this

*Corresponding author (michael.schimp@rwth-aachen.de)

Preprint submitted to Astroparticle Physics

©2016. This manuscript version is made available under the *CC-BY-NC-ND 4.0 license*
<http://creativecommons.org/licenses/by-nc-nd/4.0/> November 3, 2021

all-flavor flux has been confirmed by the measurement of an excess of uncontained up-going muons [4] at high energies above the background originating from interactions of atmospheric neutrinos. These muons are produced by charged current interactions of muon neutrinos in the ice, where the direction of the muon and the neutrino agree well within $\sim 1^\circ$ in the considered energy range. Muons propagate large distances through the ice, and can be measured with good angular resolution, i.e. $< 1^\circ$. Though such events are ideally suited for the identification of the sources, neither searches for angular autocorrelations of neutrino arrival directions nor correlations of neutrino arrival directions with the positions of known astrophysical sources have resulted in a significant observation [3, 5]. In conclusion, the total number of sources of the observed flux is presumably large as so far the individual sources have been too weak to be detectable with respect to the atmospheric neutrino background.

1.2. Angular correlations of neutrino arrival directions

This paper focusses on the non-observation of an angular correlation within 108 310 up-going muons in IceCube data measured from 2008 to 2011 with the detector configurations *IC40*, *IC59* and *IC79* [5]. That result was obtained based on two analyses. The first is a binned correlation analysis and the second uses the power coefficients of a multipole expansion of the sky map of detected neutrino arrival directions. In this work, we focus on the second result. Here, weak sources, constituting the signal, were assumed to be isotropically distributed over the sky. The signal was benchmarked according to different signal hypotheses, characterized by three quantities: the total *number of sources* in the full sky N_{Sou} , a universal *strength* of each source μ , and the *spectral index* γ of the energy spectrum. The parameter μ is the mean number of measured neutrinos per source at the horizon. While at the horizon the detection efficiency is largest, each source off the horizon is assigned a lower number of neutrinos according to the declination dependent detector acceptance.

The analysis from [5] uses a test statistics (TS) that denotes how significantly the angular correlations of muon directions in the specific skymap are distinguishable from the random atmospheric background. The expected TS shift for signal with respect to the TS expectation for pure atmospheric background in units of the standard deviation of the background TS is called *signalness* Σ in the following. In Figure 1, the TS distributions for signal hypotheses with different values for N_{Sou} are shown. The distributions are obtained by simulations of random skymaps using the information from [5] about the point spread function and zenith-dependent detector acceptance.

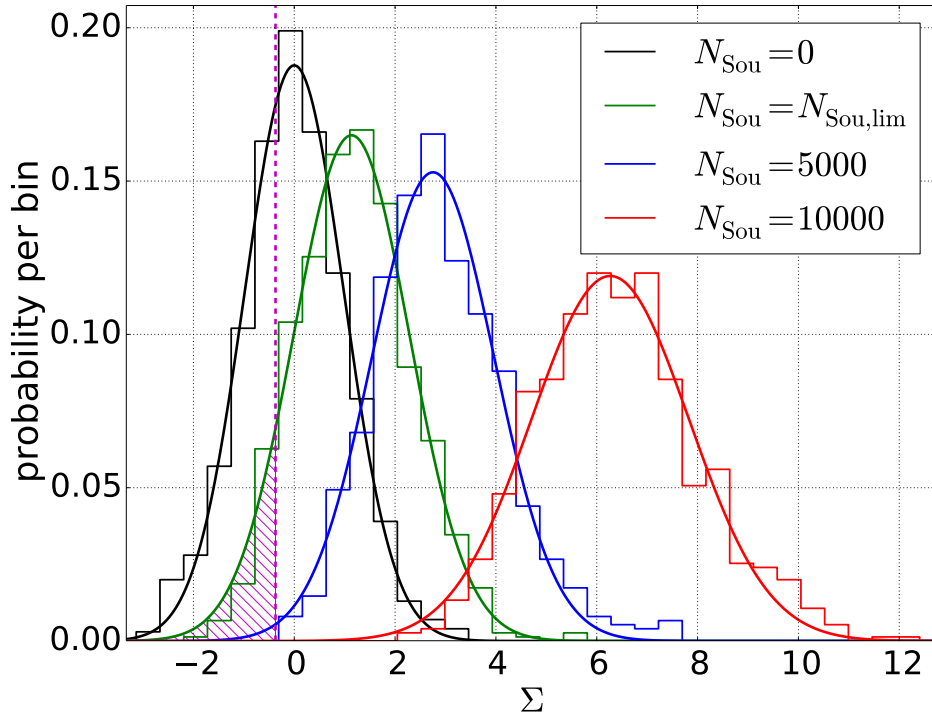


Figure 1: Distributions of the test statistic (TS) for different numbers of sources in the full sky N_{Sou} , fixed source strength $\mu = 3$ and energy spectrum $\gamma = 2.5$; dashed vertical line: result from the experimental skymap $\Sigma_{\text{exp}} = -0.3$ [5]; hatched area: lower 10% quantile of the TS distribution for a signalness $\Sigma_{\text{lim}} = 1.07$ corresponding to observed the upper limit.

We find that for a fixed source strength the signalness, i.e. the mean of the TS distribution, scales $\propto N_{\text{Sou}}$. In Figure 2, the signalness per source is shown as a function of the source strength μ . We find that the signalness per source increases with stronger sources consistently with $\frac{d\Sigma}{dN_{\text{Sou}}} \propto \mu^2$, independent of the assumed energy spectrum.

The experimentally observed value is $\Sigma_{\text{exp}} = -0.3$ [5]. The corresponding exclusion limits on the number of sources $N_{\text{Sou}} = N_{\text{Sou,lim}}$ for different values of μ are obtained from simulations as those values of N_{Sou} for which 90% of experiments would result in a larger signalness than the observed Σ_{exp} . We find that for all different combinations of N_{Sou} and μ this results in the same signalness Σ , while the variance of the TS distribution is identical. Correspondingly, the median signalness corresponding to the observed upper limit is $\Sigma_{\text{lim}} = 1.07$ and does not depend on the specific choice of

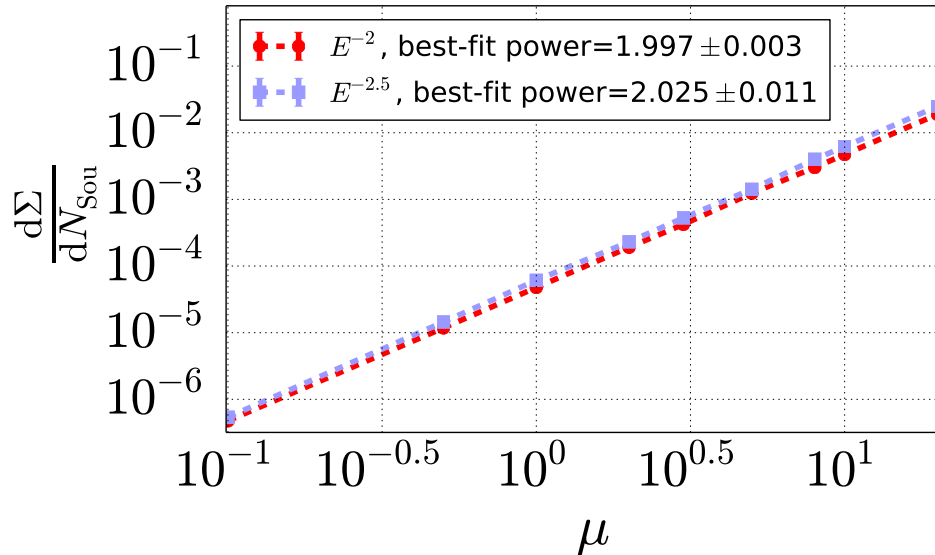


Figure 2: Signalness per source $\frac{d\Sigma}{dN_{\text{Sou}}}$ against source strength μ for astrophysical energy spectra E^{-2} and $E^{-2.5}$; legend: exponent of best-fit power law.

signal parameters. Thus, $N_{\text{Sou,lim}}$ is expressed as a simple function of the source strength μ .

1.3. Purpose of this work

Purpose of this work is to re-interpret the given exclusion limits for the number of sources of a fixed source strength in terms of astrophysically motivated distributions of source strengths $\frac{dN_{\text{Sou}}}{d\mu}$. To do this, we calculate the expected signalness as a function of the respective astrophysical model parameters and compare this to the experimentally excluded signalness. For this, we make use of the dependencies of the signalness on the model parameters N_{Sou} and μ as introduced above. As benchmark scenarios, we use two astrophysical models. For the first model, we assume isotropically distributed sources with a number density following the red-shift dependent evolution of active galactic nuclei (AGNs). For the second model, we assume an isotropic distribution of sources with strengths analogous to the strengths of extragalactic sources of high-energy photons as observed by the Fermi-LAT satellite. Further details of the models that were taken into account in this work are given in Section 2.1.

Additionally, we take into account the measured diffuse astrophysical muon neutrino flux from the Northern hemisphere [4] in order to further

constrain the scenarios. For both of the mentioned models, we test two astrophysical neutrino energy spectra $\propto E^{-\gamma}$ that are compatible with this measurement. That is a hard spectral index of $\gamma = 2.0$ and a soft spectral index of $\gamma = 2.5$.

It should be noted that other interpretations of a diffuse astrophysical neutrino flux—before and after the measurement by IceCube—have been published. These include different approaches as, for example, the interpretation of diffuse and/or stacking limits in terms of different production mechanisms [12] or the presence of point sources and their neutrino power density [25]. One recent approach is to constrain the presence of sources that are obscured in gamma rays but well visible in neutrinos such as choked GRBs [21]. Our approach differs from these in the manner that we additionally (and, in fact, primarily) interpret the absence of angular correlations in neutrino directions rather than the diffuse astrophysical flux. Taking this flux into account to further constrain our parameters of interest is technically just an optional addition but is still meaningful due to the relevance of this flux measurement. Also, while we apply our approach to specific source scenarios in this work, the method we present is generally applicable for other scenarios.

2. Method

2.1. Calculation of the source count distributions

2.1.1. Cosmologically distributed sources

For the application to sources motivated by the cosmological evolution of AGN, we assume standard sources that exhibit the same muon neutrino luminosity L in the energy range from 100 GeV to 100 TeV used in the IceCube angular correlation analysis. Due to red-shift of energy this leads to a red-shift dependency of the energy range that is used for the luminosity normalization. Using L , the source strength μ can be expressed in dependence on the cosmological redshift z :

$$\mu(z) = \frac{L}{4\pi d_L^2(z) \cdot (1+z)^{\gamma-2}} \cdot b(\gamma) \quad (1)$$

where $d_L(z)$ is the luminosity distance. The factor

$$b(\gamma) = \frac{\sum_{\text{IC}} T^{\text{IC}} \int_{100 \text{ GeV}}^{100 \text{ TeV}} dE A_{\text{eff}}^{\text{IC}}(E) E^{-\gamma}}{f(\gamma) \cdot \int_{100 \text{ GeV}}^{100 \text{ TeV}} dE E^{1-\gamma}} \quad (2)$$

takes into account the observational parameters where T^{IC} denotes the live-time of IceCube for the operation of each detector configuration IC and $A_{\text{eff}}^{\text{IC}}(E)$ is the declination-averaged effective area of each configuration IC. The factor $f(\gamma)$ is the declination-averaged detector acceptance divided by the detector acceptance at the horizon. It compensates the usage of the declination-averaged effective area $A_{\text{eff}}^{\text{IC}}$ in order to obtain the expected number of neutrinos per source at the horizon μ instead of a declination-averaged expected number of neutrinos per source. The values for $f(\gamma)$ are 0.624 and 0.848 for energy spectra with $\gamma = 2.0$ and $\gamma = 2.5$, respectively.

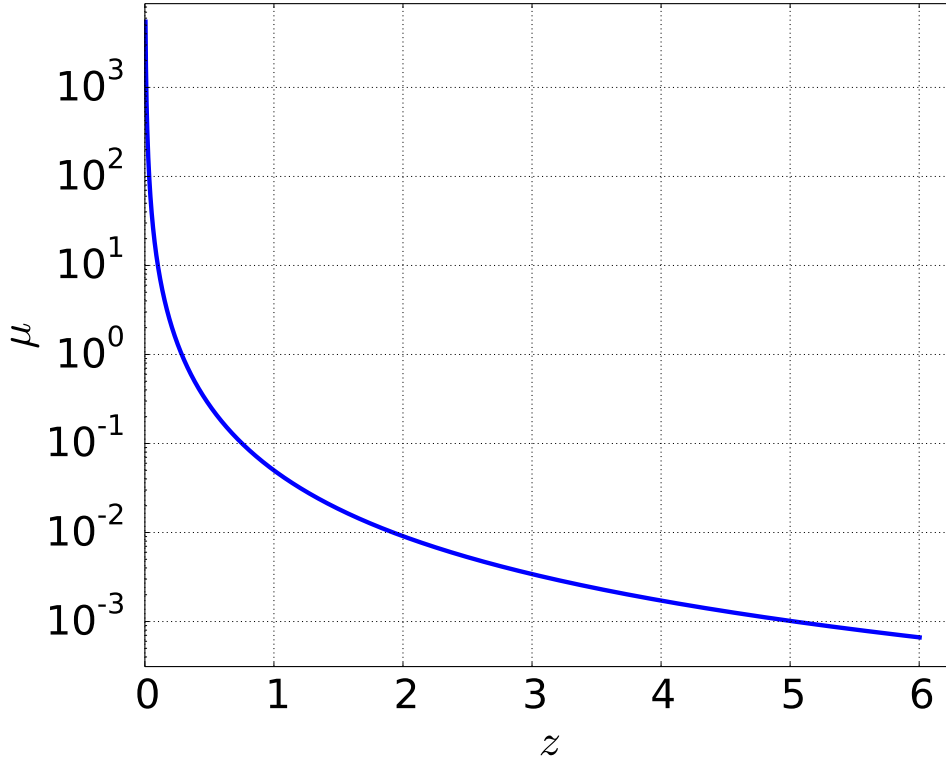


Figure 3: Redshift-dependent source strength $\mu(z)$ for sources with universal muon neutrino source luminosities $L = 7 \cdot 10^{44} \frac{\text{erg}}{\text{s}}$ and energy spectra with $\gamma = 2.0$

The luminosity distance $d_L(z)$ and the co-moving volume $V_c(z)$, are calculated using the cosmology calculator described in [27]. For this, the following cosmological parameter values are assumed [22]: $\Omega_m = 0.315^{+0.016}_{-0.017}$, $\Omega_r = 8.53 \cdot 10^{-5}$ and $\Omega_\Lambda = 0.685^{+0.017}_{-0.016}$. The given errors are propagated for a cross check: The resulting relative errors for the total number of measured

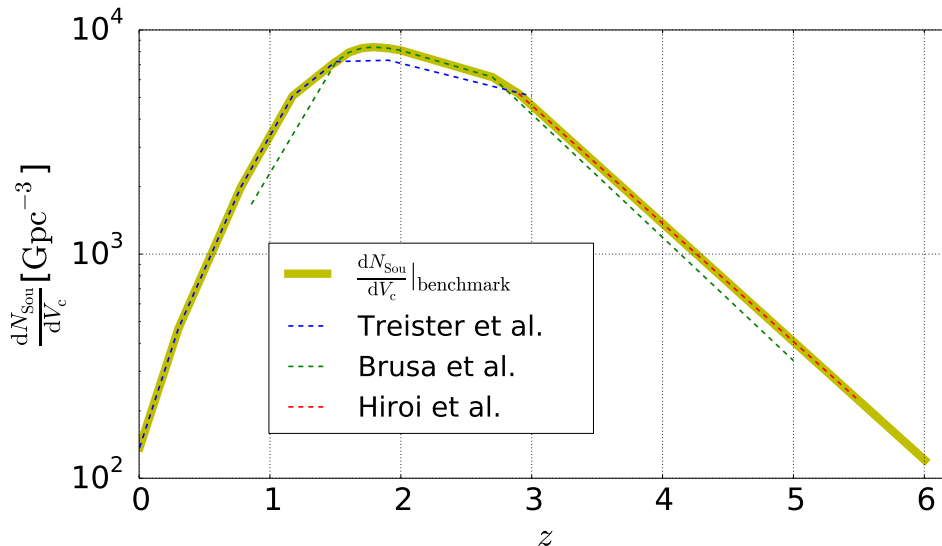


Figure 4: Yellow solid line: combined redshift-dependent co-moving source density representing AGN densities up to $z = 6$ [26, 13, 18], i.e. $\frac{dN_{\text{Sou}}}{dV_c}|_{\text{benchmark}}$; dashed lines: contributions from the articles given in the legend; kinks originate from the provision of the density distributions as interval-wise power laws

neutrinos $n(\text{scd})$ and the signalness Σ are $\sim 2.3\%$ and 1.8% , respectively. They are not regarded further as they have very little impact on the results (see for comparison the scale of α in Figure 7). In Figure 3, an exemplary distribution for $\mu(z)$ is given.

To account for the evolution of sources, a redshift-dependent co-moving source density $\frac{dN_{\text{Sou}}}{dV_c}(z)$ has to be assumed. As a benchmark the distribution $\frac{dN_{\text{Sou}}}{dV_c}|_{\text{benchmark}}$ is constructed by combining the distributions given in: [26], [13] and [18]. These individual distributions are shown as dashed lines in Figure 4. They are fits to models, representing the redshift-dependent co-moving density of high luminosity AGN above X-ray luminosity thresholds of $\sim 10^{44} \frac{\text{erg}}{\text{s}}$ up to high redshifts. The resulting distribution is represented by the yellow wide line in Figure 4. The redshift of the closest known AGN in the Northern Sky (M87) [10] is 0.004, while the expected contributions to the signalness Σ and to the number of measured neutrinos $\mu(z)$ are negligible for $z > 6$. Thus, $\frac{dN_{\text{Sou}}}{dV_c}|_{\text{benchmark}}$ is set to zero for $z < 0.004$ and $z > 6$. For this work, only the shape of $\frac{dN_{\text{Sou}}}{dV_c}|_{\text{benchmark}}$ is relevant, because the absolute scale is considered as a free parameter in our calculations (see below). Therefore, the uncertainties on the absolute values of $\frac{dN_{\text{Sou}}}{dV_c}|_{\text{benchmark}}$ are not taken into

account in the following.

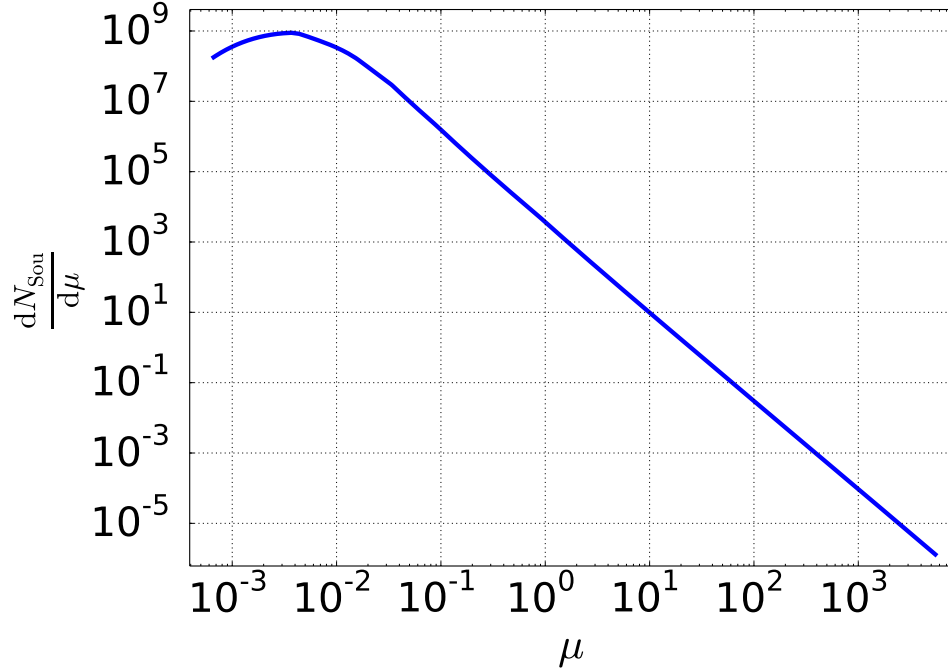


Figure 5: Source count distribution for the benchmark redshift-dependent co-moving source density distribution $\frac{dN_{\text{Sou}}}{dV_c}|_{\text{benchmark}}$ (i.e. $\alpha = 1$), $L = 7 \cdot 10^{44} \frac{\text{erg}}{\text{s}}$ and $\gamma = 2.0$

Given $\mu(z)$ and the co-moving source density $\frac{dN_{\text{Sou}}}{dV_c}$, the source count distribution is calculated by:

$$\frac{dN_{\text{Sou}}}{d\mu}(\mu) = -\frac{dz}{d\mu} \frac{dN_{\text{Sou}}}{dV_c} \frac{dV_c}{dz} \quad (3)$$

In Figure 5, the resulting source count distribution is shown for our benchmark model $\frac{dN_{\text{Sou}}}{dV_c}|_{\text{benchmark}}$.

Besides the universal muon neutrino luminosity L , a scale factor α for the source density is used as a second model parameter

$$\frac{dN_{\text{Sou}}}{dV_c} = \alpha \frac{dN_{\text{Sou}}}{dV_c}|_{\text{benchmark}} \quad (4)$$

Thus, constraining or predicting a certain value of α is equivalent to constraining or predicting the normalization of the source density distribution. As a consequence, α can be interpreted as a relative fraction of AGN described by the benchmark source density $\frac{dN_{\text{Sou}}}{dV_c}|_{\text{benchmark}}$ which contribute to the observed signal.

2.1.2. Fermi-LAT extragalactic sources

The gamma ray telescope Fermi-LAT has measured the photon flux of extragalactic high-energy photon sources with a fitted average energy spectrum of $E^{-2.4}$ in the energy range from 100 MeV to 100 GeV in a high-latitude survey [6]. It is parametrized by a broken power law:

$$\frac{dN_{\text{Sou}}}{dS}(S) = \begin{cases} AS^{-\beta_1}, & S \geq S_b \\ AS_b^{-\beta_1+\beta_2}S^{-\beta_2}, & S < S_b \end{cases}, \quad (5)$$

where $\beta_1 = 2.49 \pm 0.12$ and $\beta_2 = 1.58 \pm 0.08$ are the powers of the source count distribution after and before the break, respectively. $A = (16.46 \pm 0.80) \cdot 10^{-14} \text{ cm}^2 \text{ deg}^{-2} \text{ s}$ is a normalization factor for $\frac{dN_{\text{Sou}}}{dS}$ and $S_b = (6.60 \pm 0.91) \cdot 10^{-8} \text{ cm}^{-2} \text{ s}^{-1}$ is the photon flux at the break of the source count distribution. In Figure 6, an illustration of the used parametrization is shown.

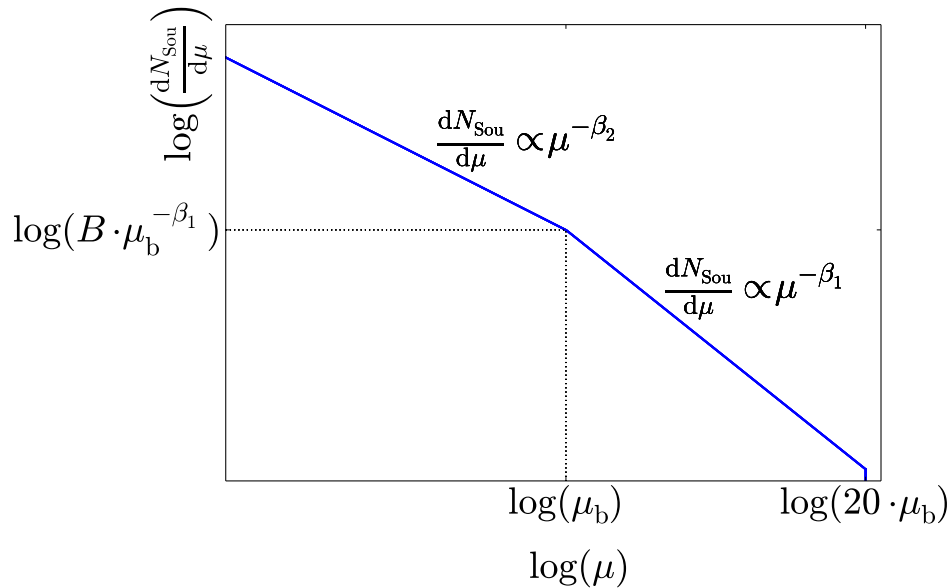


Figure 6: Sketch of the source count distribution $\frac{dN_{\text{Sou}}}{d\mu}(\mu)$ with powers β_1 and β_2 adopted from Fermi-LAT

As these photon sources are also candidates for high-energy neutrino sources [23], we adopt the parametrization as a neutrino source count distribution as explained in the following.

The photon fluxes S and S_b are replaced by the neutrino source strength μ as defined in Section 1 and the source strength at the break is denoted μ_b .

The normalization A is replaced by the dimensionless factor B . Hence, all neutrino source count distribution parameters are dimensionless in contrast to the parameters measured by Fermi-LAT. Furthermore, a cutoff is introduced by setting the source count distribution to zero for all source strengths above a maximum μ_{\max} to avoid divergences in the signalness calculation. The cutoff is fixed to $\mu_{\max} = 20\mu_b$ corresponding to the brightest source in the Fermi-LAT sample which has a flux of $S_{\max} \approx 20S_b$ [6]. This results in the following parametrization for the neutrino source count distribution:

$$\frac{dN_{\text{Sou}}}{d\mu}(\mu) = \begin{cases} 0, & \mu \geq 20\mu_b \\ B\mu^{-\beta_1}, & 20\mu_b > \mu \geq \mu_b \\ B\mu_b^{-\beta_1+\beta_2}\mu^{-\beta_2}, & \mu < \mu_b \end{cases} \quad (6)$$

The best-fit values for the powers of the Fermi-LAT source count distribution, $\beta_1 = 2.49$ and $\beta_2 = 1.58$, are initially also applied for the neutrino source count distributions before we study more general values in Section 4.3.

Though motivated by the Fermi-LAT observations, there is no a-priori correct conversion between the parameters describing the neutrino and photon source distributions, (μ_b, B) and (S_b, A) . In particular, the sensitive energy ranges for the Fermi-LAT high-latitude survey, 100 MeV–100 GeV, and for the IceCube measurement, 100 GeV–100 TeV, differ. However, as a benchmark we assume a universal neutrino-to-photon ratio $\varepsilon_{\nu/\gamma}$ for the flux received from these sources. This ratio is assumed to be constant for all energies and for all sources of the given population. One should note that several processes at the sources like inverse Compton scattering, bremsstrahlung and proton-synchrotron radiation might introduce a bias to this ratio because they affect the correlation of photon and neutrino production in an energy dependent way [28, 15, 20].

Using our assumption of a universal $\varepsilon_{\nu/\gamma}$, different values of $\varepsilon_{\nu/\gamma}$ scale the neutrino flux per source by the same factor for each source. Thus, they also scale the source strength μ of each source by the same factor $\varepsilon_{\nu/\gamma}$ and the source count distribution can still be parametrized by the broken power law given in Equation (6).

To relate the universal neutrino-to-photon ratio to the source count distribution parametrization from Fermi-LAT, first the values of (μ_b, B) for $\varepsilon_{\nu/\gamma} = 1$ are determined which are called $(\mu_{b,\text{Fermi}}, B_{\text{Fermi}})$ in the following.

They are calculated by:

$$\mu_{\text{b,Fermi}} = a(\gamma) \cdot 1000^{1-\gamma} \cdot S_{\text{b}} \quad (7)$$

$$B_{\text{Fermi}} = (a(\gamma) \cdot 1000^{1-\gamma})^{\beta_1-1} \cdot A \quad (8)$$

$$a(\gamma) = \frac{\sum_{\text{IC}} T^{\text{IC}} \int_{100 \text{ GeV}}^{100 \text{ TeV}} dE A_{\text{eff}}^{\text{IC}} E^{-\gamma}}{f(\gamma) \int_{100 \text{ GeV}}^{100 \text{ TeV}} dE E^{-\gamma}}, \quad (9)$$

where $a(\gamma)$ is the factor converting a particle flux into the observed source strength μ . The factors of $1000^{1-\gamma}$ in Equations (7) and (8) take into account the different energy ranges of Fermi-LAT and IceCube for the assumed energy spectra.

For each value of $\varepsilon_{\nu/\gamma} \neq 1$, the source strength μ of each source in the population with $B = B_{\text{Fermi}}$ and $\mu_{\text{b}} = \mu_{\text{b,Fermi}}$ has to be multiplied by $\varepsilon_{\nu/\gamma}$. For the source count distribution parameters B and μ_{b} , this leads to:

$$B = \varepsilon_{\nu/\gamma}^{\beta_1-1} \cdot B_{\text{Fermi}} \quad \text{and} \quad \mu_{\text{b}} = \varepsilon_{\nu/\gamma} \cdot \mu_{\text{b,Fermi}} \quad (10)$$

Note that we do not explicitly assume any absorption effects for the photons observed by Fermi-LAT with respect to the neutrinos observed by IceCube. However, this issue is implicitly addressed in Section 4.3 where variations in β_1 and β_2 can partly account for corresponding effects.

2.2. Limit conversion

For the interpretation of the limits from the angular correlation analysis two quantities are equated: the signalness corresponding to the limit from the angular correlation analysis and the signalness of the source population of interest, given on the right hand side of Equation (11):

$$\Sigma_{\text{lim}} \stackrel{!}{=} \int_0^{\infty} d\mu \frac{dN_{\text{Sou}}}{d\mu}(\mu) \frac{d\Sigma}{dN_{\text{Sou}}}(\mu) \quad (11)$$

The signalness of the source population is the integral of the signalness per source $\frac{d\Sigma}{dN_{\text{Sou}}}(\mu)$ as function of the source strength μ weighted with the source count distribution $\frac{dN_{\text{Sou}}}{d\mu}(\mu)$. Solving Equation (11) for parameters of an assumed source count distribution results in limits on these parameters based on the non-observation of angular correlations. Note that a methodically

similar analysis of gamma ray sources measured with Fermi-LAT is presented in [14].

The above conversion is based on the following reasoning. We assume that the positions of sources in the sky are not correlated on the scale of the angular resolution of $\lesssim 1^\circ$ and contribute independently to the observed signalness. This results in a linear dependence of the total signalness on the number of sources. As intuitively expected for an auto-correlation, the dependency of the signalness per source on the source strength is non-linear and follows a power law with a power index of 2. Both dependencies have been verified by simulations as discussed in Section 1.

2.3. Astrophysical flux normalization

The total normalization of the up-going diffuse astrophysical muon neutrino flux has been measured by IceCube [4], and can be used to additionally constrain the parameters of a source count distribution. For this, the total number of measured signal neutrinos expected from the source count distribution $n(\text{scd})$ and the corresponding number expected from the observed flux $n(\text{astro})$ are equated:

$$n(\text{scd}) = \int_0^\infty d\mu \mu \cdot f(\gamma) \cdot \frac{dN_{\text{Sou}}}{d\mu}(\mu) \stackrel{!}{=} n(\text{astro}) = \sum_{\text{IC}} T^{\text{IC}} \int_0^\infty dE A_{\text{eff}}^{\text{IC}} \cdot \frac{d\Phi}{dE}, \quad (12)$$

where $\frac{d\Phi}{dE}$ is the differential astrophysical neutrino flux as observed by IceCube. The parameter values solving Equation (12) represent maximum astrophysical scenarios that are consistent with the observation, i.e. assuming no other sources contributing to the observed flux.

3. Application to isotropic generic sources

3.1. Limit conversion and astrophysical flux normalization

In this section, the source count distribution parametrization from Section 2.1.1 is used to solve Equations (11) and (12) for (L, α) for both considered energy spectra. The solutions of Equation (11) are functions $\alpha(L)$ representing the converted upper limits on these parameters. They are shown as colored dashed lines in Figure 7.

The solutions of Equation (12) are functions $\alpha(L)$ representing the observed astrophysical flux for these parameters. They are represented as colored solid lines in Figure 7.

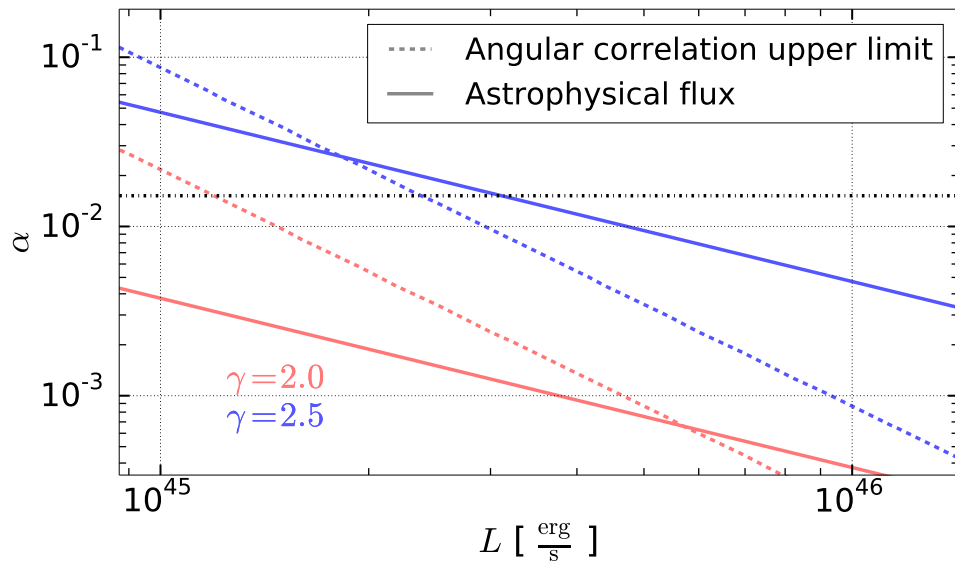


Figure 7: Results of the application to redshift-dependent comoving source densities; dashed lines: IceCube angular correlation upper limits converted to $\alpha(L)$; solid lines: $\alpha(L)$ representing the observed upgoing astrophysical muon neutrino flux; dashed-dotted line: solid angle for zenith angles between 0° and 10° divided by the solid angle of a hemisphere

The values for L at the intersections between the lines of equal colors in Figure 7 are the upper limits on the muon neutrino luminosity L under the condition that the considered source populations produce the diffuse astrophysical neutrino flux. Therefore, all larger values for L are excluded under this condition. However, for the co-moving densities, represented by the scale factor α , this is not the case: The values for α at the intersections can be exceeded under the condition that the luminosity L of each source is lower than at the intersections. This is further discussed in Section 5.1.

As introduced, a certain value of α can be interpreted as a fraction of all AGNs up to $z = 6$, i.e. a fraction of $\frac{dN_{\text{Sou}}}{dV_c}|_{\text{benchmark}}$. The value for α at the horizontal dashed-dotted line in Figure 7 is a rough estimation of the blazar fraction among the AGNs represented by $\frac{dN_{\text{Sou}}}{dV_c}|_{\text{benchmark}}$. The estimation is based on the assumption that an AGN is identified as a blazar if the angle between the AGN's jet and the viewing direction is below 10° [8]. For random orientations of jet directions the corresponding fractional solid angle is $1 - \cos(10^\circ) \approx 0.015$.

3.2. Impact of luminosity distributions

The assumption of fixed source luminosities L within a population is not realistic. Extended investigations could assume more realistic luminosity distributions or varying neutrino production efficiencies. They would, however, involve more model parameters. Our values L are to be considered as the 'effective' L of a population.

In the following, a possible type of muon neutrino luminosity distributions $\frac{dn}{dL}$ that correspond to a certain effective L , is motivated and investigated. For this, a luminosity distribution based on observations of radio galaxies at a frequency of 325 MHz is adopted from [24]. Assuming the shape of the distribution being the same for muon neutrino luminosities, its parametrization can be adopted for $\frac{dn}{dL}$. While the shape is determined this way, the normalization of $\frac{dn}{dL}$ is arbitrary for our purposes since we only consider the mean flux and mean signalness of the sources in the distribution to compare it to a given effective luminosity L . However, the actual normalization of the number density of sources of a population is still solely determined by the co-moving source density $\frac{dN_{\text{Sou}}}{dV_c}$. Thus, we obtain the two distributions shown in Figure 8 that differ only by a horizontal shift. The first represents a source distribution with the same mean flux per source as the effective luminosity $L = 7 \cdot 10^{44} \frac{\text{erg}}{\text{s}}$ used as reference. It is shown as a solid line in Figure 8. The second represents a source distribution with the same mean signalness per source as the effective luminosity mentioned above. It is shown as a dashed line in Figure 8. As

expected, the latter distribution has a lower mean luminosity because the luminous sources in this distribution are taken into account with a larger weight compared to the distribution with the same mean flux. Depending on the quantity of interest—flux or signalness of a certain population—for both of these distributions, $L = 7 \cdot 10^{44} \frac{\text{erg}}{\text{s}}$ can be considered as an effective luminosity. Moreover, analogously to the given example of Figure 8, one can obtain distributions $\frac{dn}{dL}$ using the parametrization from [24] for all effective luminosities L of interest. This allows to examine more realistic luminosity distributions corresponding to both the observed astrophysical neutrino flux and the converted angular correlation limit, represented by their effective luminosities L as given in Figure 7.

One should note, that we did not take into account the redshift dependence of the distribution $\frac{dn}{dL}$. This is due to only dependencies at low redshifts being addressed in [24], which is insufficient for the method presented here. Additionally, we assumed a redshift evolution of the source densities (see e.g. Figure 4), while the redshift dependence of the luminosity distribution in [24] holds only for the assumption of no source density evolution. Therefore, these assumptions could not be combined easily in a self consistent way. However, the additional correction from the explicit redshift dependence would only be noticeable for high redshifts for which the impact on our results is low. In conclusion, while we present our results for the simplified case of an effective luminosity L , realistic luminosity distributions $\frac{dn}{dL}$ can be mapped towards this effective luminosity as shown for the example of the parametrization given in [24]. Thus, also more sophisticated astrophysical models can be constrained by the combination of angular correlations and the observed astrophysical neutrino flux.

4. Application to Fermi-LAT extragalactic sources

In the following, the angular correlation limit and the astrophysical flux normalization are interpreted in terms of the Fermi-LAT source count distribution parameters. Then, values for a universal neutrino-to-photon ratio $\varepsilon_{\nu/\gamma}$ corresponding to the upper limit and the astrophysical flux normalization are determined. As a last step, we also determine values for $\varepsilon_{\nu/\gamma}$ corresponding to the upper limit and the astrophysical flux normalization while varying the source count distribution parameters β_1 and β_2 . By this, we constrain the possible values that β_1 and β_2 might have for neutrinos.

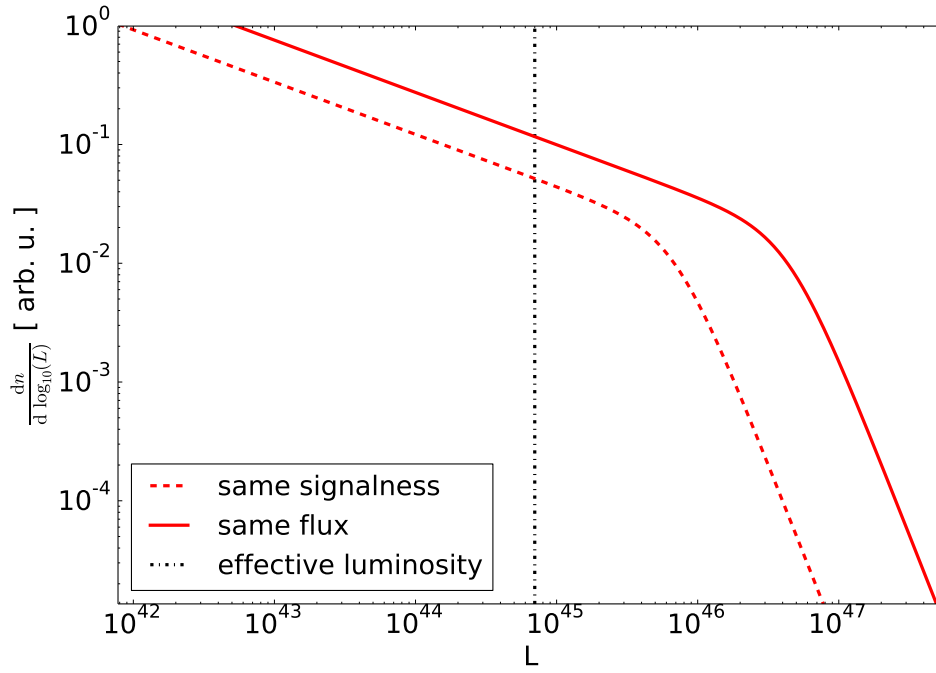


Figure 8: Exemplary muon neutrino luminosity distributions with, respectively, the same mean signalness and same mean flux per source as the effective luminosity from Figure 3; dashed line: distribution with the same mean signalness; solid line: distribution with the same mean flux; dashed-dotted vertical line: $L = 7 \cdot 10^{44} \frac{\text{erg}}{\text{s}}$ (same luminosity as in Figure 3)

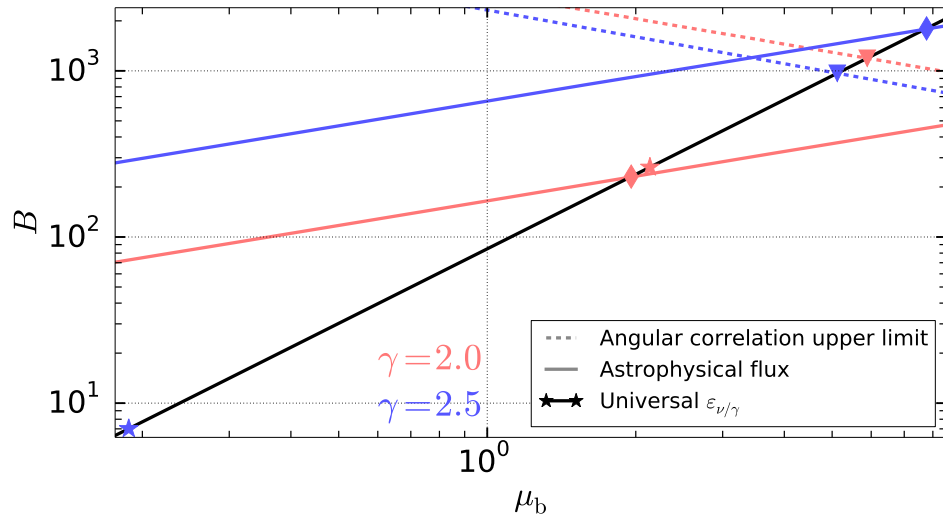


Figure 9: Dashed lines: IceCube limits for both spectral indices converted to $B(\mu_b)$; colored solid lines: values of (μ_b, B) reproducing the observed astrophysical neutrino flux; black line: values of (μ_b, B) that correspond to a universal value $\varepsilon_{\nu/\gamma}$; triangles: values of (μ_b, B) at the IceCube limit that correspond to a universal value $\varepsilon_{\nu/\gamma}$; diamonds: values of (μ_b, B) that reproduce the observed astrophysical neutrino flux and correspond to a universal value $\varepsilon_{\nu/\gamma}$; asterisks: $(\mu_{b,\text{Fermi}}, B_{\text{Fermi}})$, i.e. values such that $\varepsilon_{\nu/\gamma} = 1$.

γ	$\varepsilon_{\nu/\gamma}$	flux normalization	$\varepsilon_{\nu/\gamma}$ correlation limit	ratio
2.0		0.92	2.76	0.33
2.5		41.4	27.3	1.52

Table 1: Results for universal $\varepsilon_{\nu/\gamma}$; 2nd column: $\varepsilon_{\nu/\gamma}$ values assuming the observed neutrino flux; 3rd column: $\varepsilon_{\nu/\gamma}$ upper limits; 4th column: ratio between $\varepsilon_{\nu/\gamma}$ astrophysical flux value and $\varepsilon_{\nu/\gamma}$ upper limit

4.1. Limit conversion and astrophysical flux normalization

The solution of Equation (11) with $\frac{dN_{\text{Sou}}}{d\mu}(\mu)$ from Equation (6) is a function $B(\mu_b)$. It represents the upper limit from the angular correlation analysis [5] on B for each value of μ_b and is shown as a dashed line for each spectral index in Figure 9. The negative slopes of these lines originate from the increased signalness for larger μ_b (see Equation (11)) due to a corresponding larger non-zero integration range. This increased signalness is compensated by lower values for B , causing the negative slope.

The astrophysical flux solutions for both neutrino energy spectra are shown as solid colored lines in Figure 9. They differ because the effective area and the flux normalization in Equation (12) are energy dependent [5, 4]. Their intersections with the dashed limit lines (of the respective energy spectrum) separate the allowed region (below) from the excluded region (above) of parameter values. This means, a source population with larger values of B or μ_b cannot produce the observed flux of astrophysical muon neutrinos due to the absence of angular correlations associated with them.

4.2. The Fermi-LAT best-fit value and the neutrino-to-photon ratio

The solution $(\mu_{b,\text{Fermi}}, B_{\text{fermi}})$, corresponding to the special case of $\varepsilon_{\nu/\gamma} = 1$, is determined according to Equations (7) and (8). It is shown as an asterisk in Figure 9 for each energy spectrum. All solutions for pairs of (μ_b, B) that correspond to different universal values $\varepsilon_{\nu/\gamma} \neq 1$ are determined by Equation (10) and result in the black line shown in Figure 9.

The intersections of the (dashed) limit lines and the (solid colored) lines representing the observed astrophysical neutrino flux with the black line in Figure 9 yield values for $\varepsilon_{\nu/\gamma}$ corresponding to the angular correlation limit and the diffuse astrophysical flux for both energy spectra in this simplified model. These can be read off by considering that $\varepsilon_{\nu/\gamma} = \frac{\mu_b}{\mu_{b,\text{Fermi}}}$ according to Equation (10). By reading off the values of μ_b at these intersections (triangles and diamonds in Figure 9) and $\mu_{b,\text{Fermi}}$ (asterisks in Figure 9), one thus obtains the values for $\varepsilon_{\nu/\gamma}$. These are given in Table 1.

4.3. Variation of the source count distribution power indices

The used source count distribution parametrization (Equation (6)) can be generalized by varying the powers β_1 and β_2 and repeating the procedure from Sections 4.1 and 4.2. In Figure 10a and 10b, the results are shown in terms of the $\varepsilon_{\nu/\gamma}$ astrophysical flux values, while in Figure 10c and 10d the $\varepsilon_{\nu/\gamma}$ upper limit is shown for the neutrino energy spectra with $\gamma = 2.0$ and $\gamma = 2.5$. Finally, the ratios between the $\varepsilon_{\nu/\gamma}$ astrophysical flux value and the $\varepsilon_{\nu/\gamma}$ upper limit are shown in Figure 10e and 10f. Ratios larger than 1 indicate that the astrophysical neutrino flux is excluded to originate purely from the corresponding source population with 90 % C.L. based on the non-observation of angular correlations and assuming a universal $\varepsilon_{\nu/\gamma}$ in the considered energy ranges.

5. Conclusions

5.1. Angular correlations from generic AGN-type sources

The discussion of results from Section 3 is based on Figure 7. The angular correlation analysis constrains the allowed parameter space to the region below the dashed lines. However, also the observed diffuse astrophysical neutrino flux reflects an upper limit on the maximum allowed contribution by these sources and also parameter regions above the solid lines are excluded.

For a spectral index of $\gamma = 2.0$, the constraints by the non-observation of angular correlations are weaker than the observed flux except for very large muon neutrino luminosities of the sources above $L \simeq 6 \cdot 10^{45} \frac{\text{erg}}{\text{s}}$ in the considered energy range. For such sources, an angular correlation should have been observed and the fraction α of these sources to the total population of AGN is constrained. The fraction α would be at least a factor 20 smaller than the estimated fraction of blazars. For source luminosities well below $10^{45} \frac{\text{erg}}{\text{s}}$, where the population fraction of blazars coincides with the observed flux, the angular correlation analysis does not provide additional constraints.

The situation is different for $\gamma = 2.5$. Here, the non-observation of angular correlations excludes luminosities above $L \simeq 2 \cdot 10^{45} \frac{\text{erg}}{\text{s}}$ stronger than the constraint by the flux normalization does. The allowed parameter region would include an AGN fraction corresponding to the estimation for blazars, if their muon neutrino luminosity would reach such large values. Obviously, an improved exposure could allow to positively detect such sources. On the other hand the angular correlation analysis excludes that blazars are fully responsible for the observed flux as the required source luminosities $L \simeq 3 \cdot 10^{45} \frac{\text{erg}}{\text{s}}$ are excluded.

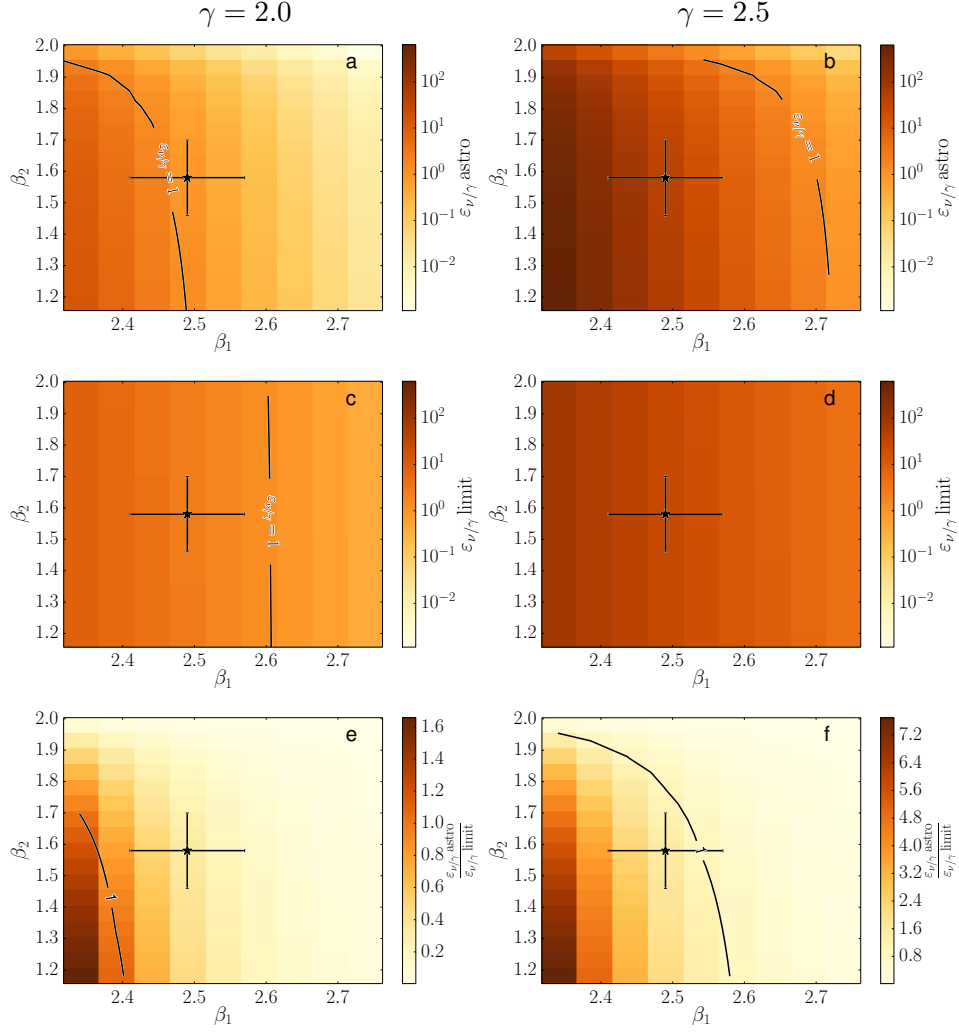


Figure 10: a, b: universal neutrino-to-photon ratios $\varepsilon_{\nu/\gamma}$ for source populations that correspond to the observed astrophysical neutrino flux for different power-indices β_1, β_2 (s. Equation (6)); c, d: converted correlation limits on an universal $\varepsilon_{\nu/\gamma}$ for different powers β_1, β_2 ; e, f: ratios between $\varepsilon_{\nu/\gamma}$ flux prediction and the $\varepsilon_{\nu/\gamma}$ limit; asterisk with error bars: β_1, β_2 and uncertainties from Fermi-LAT [6]; black line in a-c: $\varepsilon_{\nu/\gamma} = 1$; black line in e, f: ratio = 1

These conclusions depend on idealized assumptions as for example the assumption of one effective luminosity L for a whole source population. In Section 3.2 we showed that the given values for L can be interpreted in terms of specific luminosity distributions $\frac{dn}{dL}$ and showed examples of these distributions that correspond to a certain value of L . While we focused on radio sources to motivate this exemplary $\frac{dn}{dL}$, one can easily examine other parametrizations or types of luminosity distributions and interpret IceCube’s muon neutrino angular correlation limit and observed astrophysical flux in terms of these parametrizations using the method we present in this work.

In order to further interpret the effective luminosities L one can also compare them to AGN disk luminosities L_{disk} estimated in [16]. From this work, we use the L_{disk} of AGNs classified as radio loud and assume the corresponding jet luminosities L_{jet} to be 10% of L_{disk} . As our value L is the effective luminosity of a population, we take $\langle L_{\text{jet}} \rangle \approx 5 \cdot 10^{45} \frac{\text{erg}}{\text{s}}$ also as an estimate for the effective luminosity of jets. However, one should note that this estimate is conservative since the angular correlation analysis gains in sensitivity per source $\propto L^2$. Weighting sources according to L^2 leads to an effective jet luminosity $\sqrt{\langle L_{\text{jet}}^2 \rangle} \approx 9 \cdot 10^{45} \frac{\text{erg}}{\text{s}}$ which is well above the given limit on the effective luminosity. This means that it is possible to interpret our result in terms of an upper limit on $f_{\text{jet},\nu}$, which is the fraction of luminosity transferred from radio loud quasar jets into neutrinos. Specifically, for the aforementioned case that blazars constitute the detected neutrino flux with an energy spectrum of $\gamma = 2.5$, the upper limit on the effective luminosity was found to be $L \simeq 3 \cdot 10^{45} \frac{\text{erg}}{\text{s}}$. Thus, applying the effective jet luminosity of $9 \cdot 10^{45} \frac{\text{erg}}{\text{s}}$ we obtain a constraint of $f_{\text{jet},\nu} < 33\%$ for the fraction of the AGN luminosity emitted in the neutrino channel. Although, this is only a rough estimate, one should note that using this method future angular correlation analysis in IceCube might contribute significantly to constraining this fraction for more sophisticated scenarios.

5.2. Angular correlations from Fermi-LAT extragalactic sources

Unlike the modelling of generic AGN-type sources, the result here is based on an empirically observed source count distribution motivated by the observation of extragalactic high-energy gamma ray sources by Fermi-LAT. Therefore, the interpretation requires the assumption of a neutrino-to-photon ratio $\varepsilon_{\nu/\gamma}$. In order to simplify the interpretation we assume this ratio to be universal for all sources.

Starting with the results in Figure 9 and Table 1 we see that for hard spectrum sources with $\gamma = 2.0$, the observed astrophysical neutrino flux

corresponds to a lower $\varepsilon_{\nu/\gamma}$ value than the $\varepsilon_{\nu/\gamma}$ limit from the correlation analysis. Hence, for this energy spectrum, the sources from the Fermi-LAT high-latitude survey are not excluded to be the origin of the astrophysical neutrino flux under the stated assumptions. Furthermore, the flux normalization results in a required neutrino-to-photon ratio close to the generic value of $\varepsilon_{\nu/\gamma} \simeq 1$. An improved sensitivity of about a factor 3 for the correlation analysis is required to test this value. This seems well feasible with future data of IceCube.

For a softer spectrum with $\gamma = 2.5$, the opposite is the case: The required value $\varepsilon_{\nu/\gamma}$ for the astrophysical flux normalization is excluded by the $\varepsilon_{\nu/\gamma}$ limit from not observing angular correlations. This means that the astrophysical flux is excluded to be produced exclusively by sources distributed according to the Fermi-LAT motivated source count distribution parametrization for this spectrum. Furthermore, those sources would need to have neutrino-to-photon ratios of $\simeq 40$. Thus, besides their apparent absence, such high ratios would also need to be explained theoretically.

We note that the assumption of a universal $\varepsilon_{\nu/\gamma} \approx 1$ is not a robust assumption and is considered as a benchmark, only. The initial value $\varepsilon_{\nu/\gamma}$ strongly depends on the specific hadronic production mechanism, the density of the medium, as well as energy losses or acceleration of intermediate particles [17, 11, 19]. Then, depending on the optical depth of the sources, absorption of photons would lead to larger ratios [17]. However, during propagation the muon neutrino flux is also modified due to oscillations to other flavors (see e.g. [9]). In case of Fermi-Lat, the determined ratio depends on observations at largely different energy scales. It is questionable whether all sources that contribute to the Fermi-LAT source count distribution are actually dominated by photons from hadronic interactions. A strong leptonic contribution could result in substantially smaller $\varepsilon_{\nu/\gamma}$ values. As another effect, the absorption of photons during propagation is weak for the Fermi-LAT energy range affecting only the most distant sources. For the limits from the angular correlation analysis, this effect can be neglected as these are dominantly affected by the closest bright sources. Still, it would modify the total flux normalization and hence, for a fixed flux normalization, the exclusion power with respect to Fermi-LAT would be reduced. However, the obtained results provide constraints of the properties of astrophysical neutrino sources under these simplified assumptions. By including the effects discussed above, one can modify the results in order to obtain more specific constraints in terms of astrophysical source properties. For such specific modelling, the methods introduced in this work are still applicable in the same way.

Motivated by these systematic uncertainties, the studies of variations of β_1 and β_2 (s. Equations (5) and (6)) reveal several insights: First, β_1 plays a strong role for both, the $\varepsilon_{\nu/\gamma}$ astrophysical flux value and the $\varepsilon_{\nu/\gamma}$ limit because the source count distribution depends strongly on β_1 for all source strengths μ . Second, the $\varepsilon_{\nu/\gamma}$ limit is almost independent of β_2 while the $\varepsilon_{\nu/\gamma}$ astrophysical flux value noticeably depends on β_2 . This is obvious as β_2 only affects the source count distribution $\frac{dN_{\text{Sou}}}{d\mu}$ for source strengths below the break μ_b (s. Equation (6)), i.e. ‘weak’ sources.

The quantities used for the $\varepsilon_{\nu/\gamma}$ limit and the $\varepsilon_{\nu/\gamma}$ astrophysical flux value are the signalness Σ and the number of neutrinos $n(\text{scd})$ from the tested source count distribution. This leads to the conclusion that the sources brighter than μ_b , i.e. ‘strong’ sources, are the signalness dominating sources while weak sources affect only $n(\text{scd})$ and not the signalness Σ . This is a direct consequence of the definitions of $n(\text{scd})$ (Equation (12)) and Σ (Equation (11)) which depend on different powers of the source strength μ .

A ratio between a value for $\varepsilon_{\nu/\gamma}$ and the $\varepsilon_{\nu/\gamma}$ limit larger than 1 is excluded with 90 % C.L. Thus, for both energy spectra, the areas to the bottom left from the black lines in Figures 10e and 10f are excluded. For $\gamma = 2.5$, where the hypothesis with the benchmark values for β_1 and β_2 is excluded, its uncertainty interval reaches into the allowed region.

6. Summary

We have developed a method to interpret the results from analyses of angular correlations in IceCube muon neutrino data in terms of astrophysical scenarios. In addition, the observed astrophysical neutrino flux can be introduced as a boundary condition. We have shown that already with early data from the partly installed IceCube detector astrophysical scenarios can be constrained. This is especially the case for soft energy spectra. We expect a substantially improved sensitivity once results for the angular correlation with the full IceCube detector become available.

Acknowledgements

This work is supported by the Federal Ministry of Education and Research (BMBF), the Helmholtz Alliance for Astroparticle Physics (HAP) and the German Research Foundation (DFG). We thank Markus Ahlers, Jan Auffenberg, Alessandro Cuoco, Julien Lesgourgues, Leif Rädcl and Julia Tjus for the valuable discussions.

References

- [1] Aartsen, M. G. et al. (IceCube) (2013). Evidence for High-Energy Extraterrestrial Neutrinos at the IceCube Detector. *Science*, *342*, 1242856. doi:10.1126/science.1242856. arXiv:1311.5238.
- [2] Aartsen, M. G. et al. (IceCube) (2014). Observation of High-Energy Astrophysical Neutrinos in Three Years of IceCube Data. *Phys. Rev. Lett.*, *113*, 101101. doi:10.1103/PhysRevLett.113.101101. arXiv:1405.5303.
- [3] Aartsen, M. G. et al. (IceCube) (2014). Searches for Extended and Point-like Neutrino Sources with Four Years of IceCube Data. *Astrophys. J.*, *796*, 109. doi:10.1088/0004-637X/796/2/109. arXiv:1406.6757.
- [4] Aartsen, M. G. et al. (IceCube) (2015). Evidence for Astrophysical Muon Neutrinos from the Northern Sky with IceCube. *Phys. Rev. Lett.*, *115*, 081102. doi:10.1103/PhysRevLett.115.081102. arXiv:1507.04005.
- [5] Aartsen, M. G. et al. (IceCube) (2015). Searches for small-scale anisotropies from neutrino point sources with three years of IceCube data. *Astropart. Phys.*, *66*, 39–52. doi:10.1016/j.astropartphys.2015.01.001. arXiv:1408.0634.
- [6] Abdo, A. A. et al. (2010). The Fermi-LAT High-Latitude Survey: Source Count Distributions and the Origin of the Extragalactic Diffuse Background. *Astrophys. J.*, *720*, 435. doi:10.1088/0004-637X/720/1/435. arXiv:1003.0895.
- [7] Achterberg, A. et al. (IceCube) (2006). First year performance of the IceCube neutrino telescope. *Astropart. Phys.*, *26*, 155–173. doi:10.1016/j.astropartphys.2006.06.007. arXiv:astro-ph/0604450.
- [8] Ajello, M. et al. (2014). The Cosmic Evolution of Fermi BL Lacertae Objects. *Astrophys. J.*, *780*, 73. doi:10.1088/0004-637X/780/1/73. arXiv:1310.1006.
- [9] Anchordoqui, L. A. et al. (2014). Cosmic Neutrino Pevatrons: A Brand New Pathway to Astronomy, Astrophysics, and Particle Physics. *JHEAp*, *1–2*, 1–30. doi:10.1016/j.jheap.2014.01.001. arXiv:1312.6587.

- [10] Asada, K., Doi, A., Nakamura, M., Nagai, H., and Inoue, M. (2008). EVN observations of M 87. 9th EVN Symposium, Bologna.
- [11] Becker, J. K. (2008). High-Energy Neutrinos in the Context of Multimessenger Physics. *Phys. Rept.*, *458*, 173–246. doi:10.1016/j.physrep.2007.10.006. arXiv:0710.1557.
- [12] Becker, J. K. et al. (2007). Astrophysical Implications of High Energy Neutrino Limits. *Astropart. Phys.*, *28*, 98–118. doi:10.1016/j.astropartphys.2007.04.007. arXiv:astro-ph/0607427.
- [13] Brusa, M. et al. (2009). High-Redshift Quasars in the COSMOS Survey: The Space Density of $z > 3$ X-ray Selected QSOs. *Astrophys. J.*, *693*, 8. doi:10.1088/0004-637X/693/1/8. arXiv:0809.2513.
- [14] Cuoco, A., Komatsu, E., and Siegal-Gaskins, J. M. (2012). Joint Anisotropy and Source Count Constraints on the Contribution of Blazars to the Diffuse Gamma-Ray Background. *Phys. Rev.*, *D86*, 063004. doi:10.1103/PhysRevD.86.063004. arXiv:1202.5309.
- [15] Eichmann, B., Schlickeiser, R., and Rhode, W. (2012). Differences of Leptonic and Hadronic Radiation Production in Flaring Blazars. *Astrophys. J.*, *749*, 155. doi:10.1088/0004-637X/749/2/155.
- [16] Falcke, H., Malkan, M. A., and Biermann, P. L. (1995). The Jet-Disk Symbiosis. II. Interpreting the Radio/UV Correlations in Quasars. *A&A*, *298*, 375. arXiv:astro-ph/9411100.
- [17] Gaisser, T. K., Halzen, F., and Stanev, T. (1995). Particle Astrophysics with High-Energy Neutrinos. *Phys. Rept.*, *258*, 173–236. doi:10.1016/0370-1573(95)00003-Y. arXiv:hep-ph/9410384.
- [18] Hiroi, K., Ueda, Y., Akiyama, M., and Watson, M. G. (2012). Comoving Space Density and Obscured Fraction of High-Redshift Active Galactic Nuclei in the Subaru/XMM-Newton Deep Survey. *Astrophys. J.*, *758*, 49. doi:10.1086/429361. arXiv:1208.5050.
- [19] Klein, S. R., Mikkelsen, R. E., and Becker Tjus, J. (2013). Muon Acceleration in Cosmic-Ray Sources. *Astrophys. J.*, *779*, 106. doi:10.1088/0004-637X/779/2/106. arXiv:1208.2056.
- [20] Mücke, A., and Protheroe, R. (2001). A Proton Synchrotron Blazar Model for Flaring in Markarian 501. *Astropart. Phys.*, *15*, 121–136. doi:10.1016/S0927-6505(00)00141-9. arXiv:astro-ph/0004052.

- [21] Murase, K., Guetta, D., and Ahlers, M. (2015). Hidden Cosmic-Ray Accelerators as an Origin of TeV-PeV Cosmic Neutrinos. *Phys. Rev. Lett.*, *116*, 071101. doi:10.1103/PhysRevLett.116.071101. arXiv:1509.00805.
- [22] Olive, K. A. et al. (Particle Data Group) (2014). Review of Particle Physics. *Chin. Phys.*, *C38*, 090001. doi:10.1088/1674-1137/38/9/090001.
- [23] Petropoulou, M., Dimitrakoudis, S., Padovani, P., Mastichiadis, A., and Resconi, E. (2015). Photohadronic Origin of γ -ray BL Lac Emission: Implications for IceCube Neutrinos. *Monthly Notices of the Royal Astronomical Society*, *448*, 2412–2429. doi:10.1093/mnras/stv179. arXiv:1501.07115.
- [24] Prescott, M. et al. (2015). Galaxy And Mass Assembly (GAMA): The 325 MHz Radio Luminosity Function of AGN and Star Forming Galaxies. *Monthly Notices of the Royal Astronomical Society*, *457*, 730–744. doi:10.1093/mnras/stv3020. arXiv:1601.00003.
- [25] Silvestri, A., and Barwick, S. W. (2010). Constraints on Extragalactic Point Source Flux from Diffuse Neutrino Limits. *Phys. Rev. D*, *81*, 023001. doi:10.1103/PhysRevD.81.023001. arXiv:0908.4266.
- [26] Treister, E., Urry, C. M., and Virani, S. (2009). The Space Density of Compton-Thick Active Galactic Nucleus and the X-Ray Background. *Astrophys. J.*, *696*, 110. doi:10.1088/0004-637X/696/1/110. arXiv:0902.0608.
- [27] Wright, E. L. (2006). A Cosmology Calculator for the World Wide Web. *Publications of the Astronomical Society of the Pacific*, *118*, 1711–1715. doi:10.1086/510102. arXiv:astro-ph/0609593.
- [28] Zacharias, M., and Schlickeiser, R. (2012). External Compton Emission in Blazars of Nonlinear Synchrotron Self-Compton-Cooled Electrons. *Astrophys. J.*, *761*, 110. doi:10.1088/0004-637X/761/2/110. arXiv:1210.6837.